nature nanotechnology

LETTERS

PUBLISHED ONLINE: 23 FEBRUARY 2015 | DOI: 10.1038/NNANO.2015.6

Enhancement of near-field radiative heat transfer using polar dielectric thin films

Bai Song[1†], Yashar Ganjeh[1†], Seid Sadat[1†], Dakotah Thompson[1], Anthony Fiorino[1], Víctor Fernández-Hurtado[2], Johannes Feist[2], Francisco J. Garcia-Vidal[2,3], Juan Carlos Cuevas[2], Pramod Reddy[1,4*] and Edgar Meyhofer[1*]

Thermal radiative emission from a hot surface to a cold surface plays an important role in many applications, including energy conversion, thermal management, lithography, data storage and thermal microscopy[1,2]. Recent studies[3–5] on bulk materials have confirmed long-standing theoretical predictions indicating that when the gap between the surfaces is reduced to tens of nanometres, well below the peak wavelength of the blackbody emission spectrum, the radiative heat flux increases by orders of magnitude. However, despite recent attempts[6], whether such enhancements can be obtained in nanoscale dielectric films thinner than the penetration depth of thermal radiation, as suggested by theory, remains experimentally unknown. Here, using an experimental platform that comprises a heat-flow calorimeter with a resolution of about 100 pW (ref. 7), we experimentally demonstrate a dramatic increase in near-field radiative heat transfer, comparable to that obtained between bulk materials, even for very thin dielectric films (50–100 nm) when the spatial separation between the hot and cold surfaces is comparable to the film thickness. We explain these results by analysing the spectral characteristics and mode shapes of surface phonon polaritons, which dominate near-field radiative heat transport in polar dielectric thin films.

To experimentally study near-field radiative heat transfer (NFRHT) for a broad range of film thicknesses we developed an ultra-sensitive, micro-fabricated calorimetric platform that enables quantitative studies of gap-size-dependent heat currents from a spherical hot surface (the emitter) to a planar, colder surface (the receiver) (Fig. 1). Understanding NFRHT is key to developing novel technologies such as heat-assisted magnetic recording[8] and lithography[9] as well as near-field-based thermal management[10–14]. Despite long-standing theoretical predictions[2,9,15–18], only recently have measurements from bulk materials using either scanning probes with integrated thermal sensors[5] or bimaterial cantilever-based calorimeters[3,4] provided experimental support of striking enhancements in radiative heat transfer at the nanoscale. In spite of this important progress, one of the most interesting theoretical predictions, which suggests that NFRHT in nanoscale gaps is dramatically enhanced by even nanometre-thick polar dielectric films[18–21], has remained experimentally untested. In a recent experimental report[6] NFRHT was studied between a Au tip and a Au surface coated with a monolayer of NaCl, but the results were inconclusive and seemed to defy theoretical interpretation, in part because an accurate measurement of heat currents could not be carried out.

The experimental platform used in this work to study the film thickness dependence of NFRHT is shown in Fig. 1. We precisely controlled the gap size between the spherical emitter and the planar receiver to be as small as 20 nm to as large as 10 μm using a custom-built nanopositioning platform[22], while simultaneously measuring heat currents between them to obtain the thermal conductance as a function of gap size. Contact between the emitter and the receiver was optically monitored (Fig. 1a). More specifically, the emitter device (Fig. 1a) consisted of a suspended silicon region onto which a 53-μm-diameter silica (SiO_2) sphere was attached (see Methods). The emitter also featured a platinum resistance heater–thermometer through which a sinusoidal electric current ($f = 1$ Hz) was supplied to locally modulate the temperature of the suspended region and the sphere at $2f$ (Supplementary Fig. 3).

The receiver (Fig. 1a,d) was made from silicon nitride (SiN_x) and was suspended via thin, long beams to achieve a thermal conductance (G_{beams}) of ~2 μW K^{-1}. The planar suspended region was coated with SiO_2 layers of varying thickness (50 nm–3 μm), deposited on a 100-nm-thick gold film (Fig. 1b,d). The receiver also featured an integrated platinum resistance thermometer, which could resolve small temperature changes (~50 μK, in a 5 mHz bandwidth, when modulated at 2 Hz), enabling the detection of small heat currents of ~100 pW (2 μW K^{-1} × 50 μK).

Our experimental technique contributes several improvements for NFRHT measurements over previously used bimaterial cantilever-based approaches[3,4], where the deflection of the bimaterial cantilever is potentially affected by both temperature changes and forces (such as electrostatic or Casimir), posing challenges to the interpretation of experiments[23]. In contrast, in the present technique, mechanical motion (detected optically) does not affect temperature measurements that are performed independently with a resistance thermometer. Moreover, we are able to modulate the temperature of the emitter and thus employ lock-in based techniques that enhance[7] the heat flow resolution to about 100 pW.

We began measurements with receivers coated with 3-μm-thick layers of SiO_2, which we expected to behave in a manner similar to bulk devices given their comparatively large thickness. After aligning a receiver and emitter with a gap size of ~10 μm in our nanopositioning platform[22] (Fig. 1e), we moved the nanopositioner into a vacuum chamber (<10^{-6} torr, room temperature) and modulated the emitter temperature (ΔT_{emit}) sinusoidally at 2 Hz with a 10 K amplitude. The resulting radiative heat currents were quantified by measuring the temperature oscillations of the receiver (ΔT_{rec}) using the integrated resistance thermometer. To measure the gap dependence of the heat transfer we displaced the emitter

[1]Department of Mechanical Engineering, University of Michigan, Ann Arbor, Michigan 48109, USA. [2]Departamento de Física Teórica de la Materia Condensada and Condensed Matter Physics Center (IFIMAC), Universidad Autónoma de Madrid, Madrid 28049, Spain. [3]Donostia International Physics Center (DIPC), Donostia/San Sebastián 20018, Spain. [4]Department of Materials Science and Engineering, University of Michigan, Ann Arbor, Michigan 48109, USA. †These authors contributed equally to this paper. *e-mail: pramodr@umich.edu; meyhofer@umich.edu

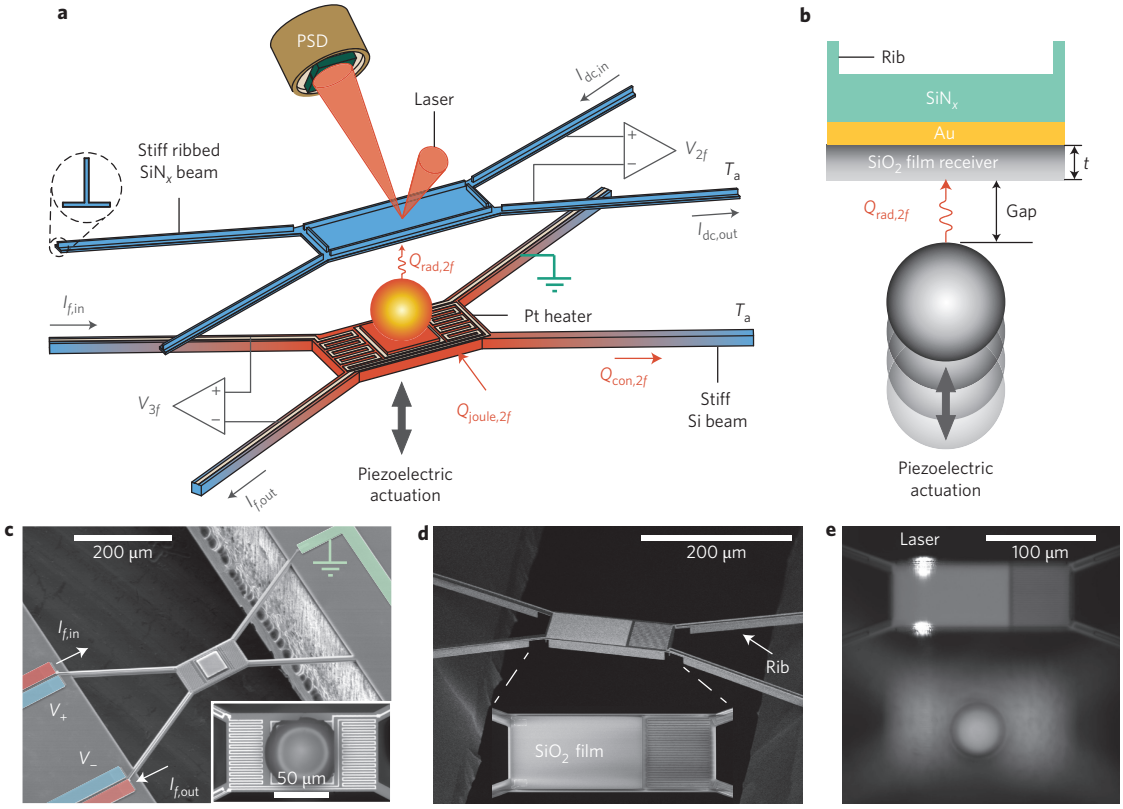

Figure 1 | Experimental set-up and devices. a, Schematic of the experimental set-up. The emitter consists of a suspended silicon platform, with an attached silica sphere and an integrated electrical heater–thermometer. The receiver is a stiff silicon nitride platform coated with gold and a silica film of suitably chosen thickness. A laser (reflected off the receiver, see also **e**) and a position-sensitive detector (PSD) enable optical detection of emitter–receiver contact formation with nanometre resolution. A sinusoidal electrical current ($I_{f,in} = I_{f,out}$), at $f = 1$ Hz, is supplied to the emitter's resistor, resulting in Joule heating with amplitude $Q_{joule,2f}$ and frequency 2 Hz. This is partly conducted through the beams ($Q_{con,2f}$) and partly radiated to the emitter ($Q_{rad,2f}$). The emitter's temperature oscillations are quantified by measuring the third harmonic of the voltage (V_{3f}) across the resistor. The receiver's temperature oscillations are measured by supplying a dc current ($I_{dc,in} = I_{dc,out}$) through the receiver's resistor and by monitoring the voltage output at $2f$ (V_{2f}) across it. T_a is the ambient temperature. **b**, Schematic cross-section of the planar receiver region and the spherical silica emitter. The gold layer is ~100 nm thick, and the thickness t of the SiO_2 film varies from 50 nm to 3 µm for different receiver devices. **c**, Scanning electron microscope (SEM) image of the suspended platform and optical image (inset) of the spherical emitter. **d**, SEM images of the receiver show ribbed beams and suspended regions. **e**, Optical image of the emitter and receiver during alignment. In this image the devices were laterally displaced to enable simultaneous visualization.

towards the receiver with a piezoelectric actuator. Nanometre-precise displacements were achieved by monitoring the movement of the actuator with integrated strain gauge sensors under closed-loop feedback control (Supplementary Fig. 6). The top panel of Fig. 2a shows the displacement, Δ_z, of the emitter towards the receiver, which begins with coarse steps (~5 nm) and continues in finer steps (~2.5 nm) close to contact. Throughout the approach the optical signal (middle panel) does not change until contact is established. Finally, the bottom panel presents ΔT_{rec}, which increases monotonically until contact is made. Contact is heralded by a sudden change in the optical deflection signal, which occurs concurrently (that is, within the same 2.5 nm displacement step) with a large jump in ΔT_{rec} due to conduction of heat from the silica sphere to the receiver.

These experimental data allowed us to determine the gap-dependent, radiative thermal conductance as $G_{gap} = G_{beams} \times \Delta T_{rec}/(\Delta T_{emit} - \Delta T_{rec})$. We obtained the near-field thermal conductance (G_{NF}) at each gap by subtracting the gap-dependent far-field contribution, which was estimated from the thermal conductance at the largest measured gap sizes (~10 µm) and the calculated gap-dependent view factor (Fig. 2b and Supplementary Fig. 7). The estimated G_{NF} for the 3-µm-thick layer of SiO_2 as a function of gap size is shown in Fig. 2c (green open circles). Clearly, G_{NF} increases rapidly from ~0 to 12 nW K^{-1} as the gap size is reduced to ~20 nm.

To investigate the effect of film thickness on NFRHT we used receivers coated with a 100-nm-thick SiO_2 layer and measured G_{NF} (Fig. 2c, green solid circles). Intriguingly, the near-field thermal conductance for these devices remains largely unchanged when the gap is reduced to well below 1 µm, and only begins to increase noticeably with gaps below 300 nm. When the gap size approaches the film thickness, G_{NF} increases rapidly and becomes comparable to that obtained for 3-µm-thick SiO_2 films at gaps less than 100 nm. To better understand the dependence of G_{NF} on SiO_2 thickness, we performed additional experiments for layer thicknesses of 50 nm, 1 µm and 2 µm (Fig. 2c, all data points represent an average of ~10 independent measurements). It is clear from these experiments that G_{NF} for each device depends on the thickness of the coating and begins to increase rapidly only when the gap size becomes comparable to the film thickness. We also performed a control experiment where the receiver had only a 100-nm-thick Au film and no SiO_2 coating. The results of this experiment (solid olive squares in Fig. 2c) show that there is no measurable increase in G_{NF} as the gap size decreases. Taken together, our observations suggest that surface phonon polaritons on the SiO_2 surfaces are responsible for the observed, gap-dependent G_{NF} behaviour.

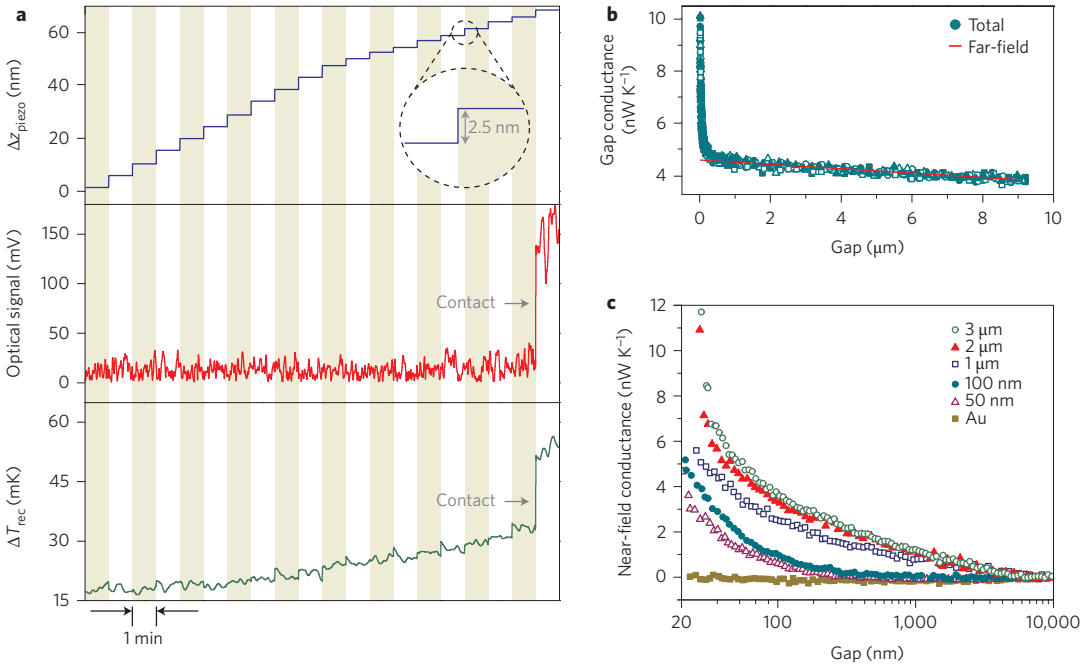

Figure 2 | Gap-dependent near-field thermal conductance of thin films. a, Simultaneous recording of displacement, Δ_z, of the emitter towards the receiver (top), optical contact signal (middle) and temperature increase in the receiver (bottom). During the final approach, piezo displacement steps of ~2.5 nm were used. **b**, Contribution of far-field radiation to the radiative thermal conductance across the gap for a representative film (100 nm). The solid red line describes the predicted far-field radiation, which increases weakly (<1 nW K^{-1}) with decreasing gap size due to the associated change in view factor. As expected, the measured data (multiple runs, green symbols) agree well with the far-field prediction for gaps from 1 to 10 μm. **c**, Near-field thermal conductance as a function of film thicknesses. Data for each film thickness represent an average of ~10 different data sets. See Supplementary Fig. 7 for information about the standard deviation of the data.

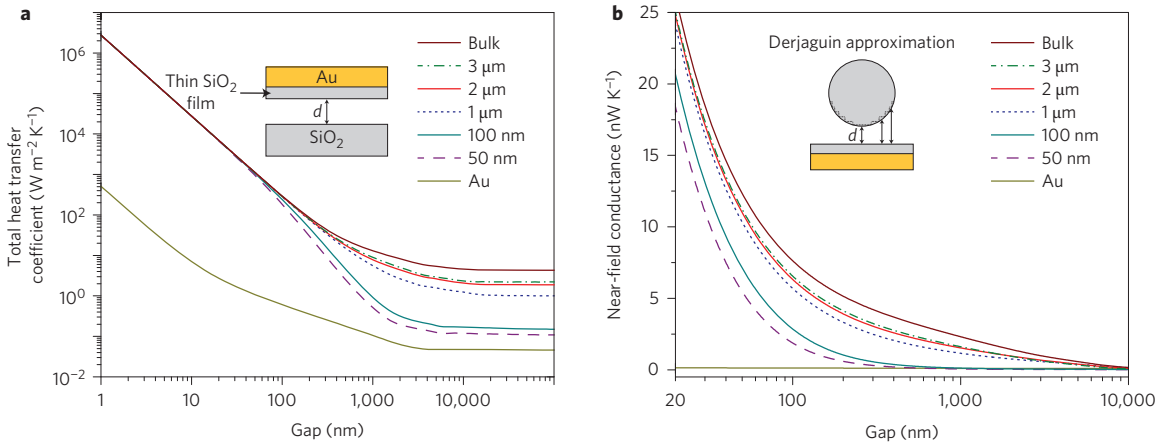

Figure 3 | Computed heat transfer coefficients. a, Computed total heat transfer coefficient as a function of gap size for the multilayer system shown in the inset. This structure comprises a thick, semi-infinite silica surface separated by a vacuum gap of size d from a silica thin film coating on a semi-infinite Au surface. Different curves correspond to different thicknesses of the silica coating. **b**, Calculated near-field conductance as a function of gap size for the sphere and coated layer system shown in the inset. The sphere has a diameter of 53 μm and the SiO_2–Au structure is assumed to be infinite in the transverse directions. Different curves correspond to different values of coating thickness. These results were obtained using the data in **a**, within the Derjaguin approximation (see Methods and Supplementary Information) and by subtracting the far-field contribution to make a direct comparison with the experiments. In all calculations the temperature was assumed to be 300 K.

We next evaluated whether our experimental findings of NFRHT in thin films are in (quantitative) agreement with theoretical predictions. Towards this end we combined the formalism of fluctuational electrodynamics[24] with a scattering matrix approach[25] (see Methods and Supplementary Section IIIA) and calculated the heat transfer coefficient (thermal conductance per unit area, h) between a semi-infinite SiO_2 surface and SiO_2 thin films coated on a semi-infinite Au surface (Fig. 3a, inset). The computed h values for multilayer structures with different coating thicknesses (50 nm–3 μm, bulk) show that heat transfer is indeed enhanced when the gap size is reduced and converges to that between bulk SiO_2 surfaces for small (<100 nm) gap sizes (Fig. 3a). To establish

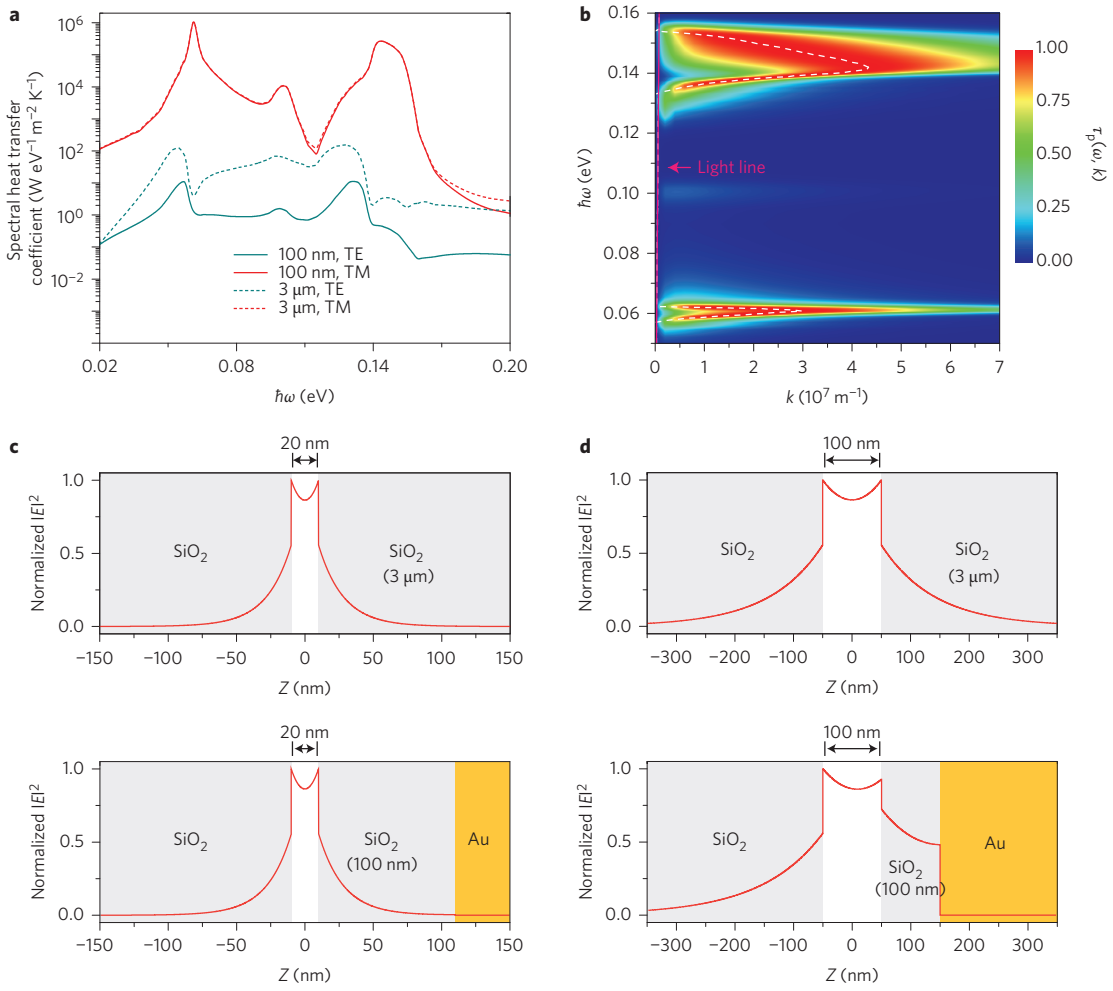

Figure 4 | Role of surface phonon polaritons in near-field radiative heat transfer. a, Spectral heat transfer coefficient for TE and TM modes as a function of radiation energy for the multilayer system in Fig. 3a with coating thicknesses of $t = 100$ nm (solid lines) and $t = 3$ μm (dashed lines) at a gap of 20 nm. The heat transfer is dominated by TM modes and their contribution is almost identical for both thicknesses. Z represents the distance from the centre of the gap. **b**, Corresponding transmission probability for TM modes, $\tau_p(\omega, k)$, as a function of radiation energy and magnitude of the parallel wavevector for $t = 100$ nm and $d = 20$ nm. The white dashed line corresponds to the analytical dispersion relation of the cavity surface phonon polaritons, and the pink solid line next to the y-axis represents the light line, that is, $\omega = kc$. The maxima of the transmission appear largely to the right of the light line and therefore correspond to evanescent waves. **c**, Normalized electric field intensity of a representative cavity surface phonon polariton (CSPhP) mode ($\hbar\omega = 61.2$ meV) for a gap of 20 nm and thicknesses of $t = 3$ μm (upper panel) and $t = 100$ nm (lower panel), normalized to peak intensity. Grey regions correspond to SiO_2 and the yellow region represents Au. **d**, As in **c**, but for a gap of 100 nm.

a direct comparison with our experimental results, we computed the near-field conductance between a 53-μm-diameter silica sphere and thin film-coated surfaces (Fig. 3b) via the Derjaguin approximation[26] (see Methods). The predicted conductances, as a function of gap size and film thickness, are in good overall agreement with our measurements (cf. Figs 2c and 3b), although the calculated conductances consistently overestimate the measured thermal conductance (see Supplementary Fig. 12 for a direct comparison). As we demonstrate in Supplementary Section IIIC and Supplementary Fig. 13, these deviations are not due to the use of the Derjaguin approximation, which provides accurate results for the NFRHT in our systems in spite of the nanometre-scale roughness of the films. Instead, we attribute this comparatively small discrepancy to the inevitable uncertainties associated with the microstructure and optical properties of the integrated thin films. Overall, the observed agreement between measurements and theoretical predictions suggests that fluctuational electrodynamics successfully captures the key aspects of the gap-dependent NFRHT in these thin-film structures and raises the key question: what is the origin of the film thickness dependence of G_{NF}?

To elucidate the origin of the thickness dependence of the NFRHT we compared (for two multilayer configurations with 100-nm- and 3-μm-thick SiO_2 films and 20 nm gaps) the calculated spectral heat transfer coefficients $h_s(\omega)$ and $h_p(\omega)$ for the transverse electric (TE) and transverse magnetic (TM) modes, respectively (Fig. 4a and Supplementary Fig. 9). It can be seen that TM modes dominate heat transfer at small gap sizes, with major contributions from two narrow energy ranges centred around ~0.06 eV and ~0.14 eV. To determine which modes dominate the heat flux we plot in Fig. 4b the transmission probability (see Methods) for the TM modes, which depends on both the frequency (ω) and the magnitude (k) of the parallel component of the wavevector. We also overlay the computed dispersion relationship for cavity surface phonon polaritons (CSPhPs, dashed line) and the light line (solid line) on this plot. It can be seen that the transmission probability is largest in the aforementioned energy ranges (Fig. 4b) and occurs for wavevectors that

lie to the right of the light line, that is, for evanescent waves. Furthermore, it can be seen that these wavevectors either overlap or lie in close vicinity to the dashed line. This strong overlap between the transmission peaks and the dashed dispersion line clearly shows that enhancements of heat transfer are primarily due to CSPhPs supported by the cavity between the SiO_2 layers.

Finally, to clarify the origin of the convergence of NFRHT for thin and thick films at small gap sizes, we note that when the gap size d is smaller than the film thickness, the dispersion of CSPhPs (including the dispersions shown in Fig. 4b and Supplementary Fig. 11) can be analytically approximated (Supplementary Section IIIB) by $k_C = (1/d)\ln((\varepsilon(\omega)-1)/(\varepsilon(\omega)+1))$, where k_C is the complex amplitude of the parallel component of the wavevector and $\varepsilon(\omega)$ is the dielectric function of SiO_2. For the surface modes that dominate the NFRHT, which are evanescent both in the vacuum and inside the silica, the penetration depth l of CSPhPs can be approximated by $[2\mathrm{Re}\{k_C(\omega)\}]^{-1}$. Thus, we find that $l \approx d$, confirming that the penetration depth is independent of the film thickness and decreases with decreasing gap size. This fact is illustrated in Fig. 4c, where we compare the normalized electric field intensity of representative CSPhP modes, corresponding to an energy of ~61.2 meV, for two coating thicknesses (100 nm and 3 μm) and a gap of 20 nm. Notice that the mode shapes are almost identical due to the small penetration depths, showing that NFRHT in small gaps occurs through identical modes for both thin and thick films and is hence unaffected[27] by film thickness or the presence of a gold layer. In contrast, when the gap becomes comparable to or larger than the film thickness, the intensity of these modes decays slowly in SiO_2, but drops sharply at the SiO_2–Au interface (Fig. 4d, lower panel), reducing their ability to contribute to heat transport and leading to a diminished transmission probability (Supplementary Fig. 10). Thus, NFRHT enhancement for thin films at gaps larger than the film thickness is significantly smaller than that of thicker films at the same gap size. Finally, we observe that the large reduction in the NFRHT in the absence of a dielectric coating is mainly due to the mismatch between the spectral coefficients of SiO_2 and Au and is consistent with past work[4]. The above analysis provides an intuitive picture that relates the NFRHT properties of thin films, which were previously understood[19,21,28] via the penetration depth of radiation, to the shape of the cavity modes. This shows that insights from plasmonics, which enable intricate control of mode shapes, can be employed to tune NFRHT in a variety of nanoscale systems.

The experimental results and analysis presented here show that NFRHT can be dramatically affected by dielectric films if the gap size is comparable to the film thickness. Our instrumentation enables NFRHT measurements with ~100 pW resolution while precisely controlling the gap size between hot and cold surfaces with nanometre resolution. We believe that these advances can enable the study of a variety of other nanoscale radiative heat transport phenomena that remain as yet experimentally unexplored[14,29]. Insights from such studies are critical for optimizing thermal management in future nanoscale devices and for realizing near-field-based lithography and thermo-photovoltaics[9,12,30].

Methods

Device geometry of the emitter and receiver. The emitter and receiver devices were fabricated using standard microfabrication processes (Supplementary Fig. 1). The suspended regions of the emitter devices were connected to the surrounding substrate via beams (Fig. 1c) with a relatively large cross-sectional area (10 μm × 10 μm), resulting in stiff devices (~500 N m^{-1}) with a thermal conductance of ~180 μW K^{-1}. The beams and suspended regions of all receivers included ribs (Fig. 1d), which also led to stiff devices (~66 N m^{-1}; see Supplementary Fig. 4 for details) with extremely flat suspended regions. Given the excellent sensitivity of the receiver we were able to resolve heat currents at emitter–receiver distances as large as 10 μm.

Characterization of emitter and receiver. Care was taken to prevent particulate contamination of the device surfaces during fabrication and preparation of the devices for experiments (Supplementary Fig. 2). Commercial silica spheres (Corpuscular Inc.) were integrated into the devices after cleaning them in deionized water to remove particulate contamination. Subsequently, spheres were manually attached to emitter devices using a micromanipulator and an adhesive (Crystalbond 509) that provides excellent thermal contact. The topography of the devices, the cleanliness of the surfaces and the planarity of the receiver device were quantified using atomic force microscopy, dark-field optical microscopy and confocal laser scanning imaging (Supplementary Fig. 5). The thermal conductance and thermal time constant of the emitter and receiver devices were characterized by experiments and/or finite-element modelling (Supplementary Fig. 3). Supplementary Section IA presents details of the fabrication and characterization of the devices.

Optical scheme for detection of contact between emitter and receiver. Accurate detection of contact between the emitter and receiver is critical for both interpreting our measurements of near-field thermal conductance as well as to precisely determine the gap size between the top of the spherical emitter and the planar surface of the receiver at intermediate steps before contact. We note that the emitter was rigidly mounted on a piezoactuator for which the displacement was controlled with ~2.5 nm resolution using strain-gauge sensors (SGSs) embedded into the piezoactuator. See Supplementary Fig. 6 for a diagram illustrating the experimental procedure and Fig. 2a for experimental data regarding step sizes.

To accurately detect contact between the emitter and receiver, the position of the emitter was sinusoidally modulated for a short period (~5 s) after each step with an amplitude of ~4 nm at a frequency of 4 kHz. Deflections of the optical beam (at 4 kHz), reflected from the back of the receiver (Fig. 1a), were monitored using a photosensitive detector and a lock-in amplifier (time constant 30 ms). As can be seen from Fig. 2b, when contact is made the output of the lock-in amplifier suddenly increases due to sinusoidal displacements of the receiver. Note that, as the emitter approaches the receiver, there is a point where the emitter is close enough to the receiver to cause 'snap-in' due to residual electrostatic charges. In the present experiments, such snap-in was reduced to very small values by the large stiffness of the devices and due to the incorporation of a grounding loop and plane for the emitter and receiver, respectively, and was experimentally quantified to be <5 nm (Supplementary Section IC). In all our experiments a two-stage temperature controller was used that minimized the temperature drift of the nanopositioner to <10 mK over the period of the experiment.

Computational techniques. NFRHT was computed within the framework of fluctuational electrodynamics[24]. The electromagnetic properties of the different materials were described via local frequency-dependent dielectric functions. The dielectric functions of SiO_2 and Au were obtained from previous works (refs 42 and 43 in the Supplementary Information). The dispersion relations of the surface phonon polaritons and their electric field profiles were computed with a scattering matrix formalism[25]. The heat transfer coefficient h was computed from the following expression[19]:

$$h = \int_0^\infty \frac{\mathrm{d}\omega}{4\pi^2}\frac{\partial[\hbar\omega/(e^{\hbar\omega/k_B T}-1)]}{\partial T}\int_0^\infty \mathrm{d}k k[\tau_s(\omega,k)+\tau_p(\omega,k)] \quad (1)$$

where T is the temperature, ω is the radiation frequency, k is the magnitude of the wavevector component parallel to the layer planes, and τ_s and τ_p are the transmission probabilities for TE and TM modes, respectively, which depend on the Fresnel coefficients of the interfaces (Supplementary Section IIIA). The near-field conductance between the silica sphere and the thin film-coated surface was computed via the Derjaguin approximation[26] (inset of Fig. 3b and Supplementary Fig. 8) in which the sphere was approximated by a series of annuli and the thermal conductance between each annulus and the corresponding region of the thin film was computed from the data in Fig. 3a and summed. Furthermore, the far-field contribution was subtracted (Supplementary Section IIIA) to obtain the near-field conductance shown in Fig. 3b. Finally, Supplementary Section IIIC provides a demonstration that the Derjaguin approximation provides accurate results for NFRHT in our system.

Received 8 August 2014; accepted 10 January 2015; published online 23 February 2015

References

1. Wilde, Y. D. *et al.* Thermal radiation scanning tunnelling microscopy. *Nature* **444,** 740–743 (2006).
2. Jones, A. C., O'Callahan, B. T., Yang, H. U. & Raschke, M. B. The thermal near-field: coherence, spectroscopy, heat-transfer, and optical forces. *Prog. Surf. Sci.* **88,** 349–392 (2013).
3. Rousseau, E. *et al.* Radiative heat transfer at the nanoscale. *Nature Photon.* **3,** 514–517 (2009).
4. Shen, S., Narayanaswamy, A. & Chen, G. Surface phonon polaritons mediated energy transfer between nanoscale gaps. *Nano Lett.* **9,** 2909–2913 (2009).
5. Kittel, A. *et al.* Near-field heat transfer in a scanning thermal microscope. *Phys. Rev. Lett.* **95,** 224301 (2005).

6. Worbes, L., Hellmann, D. & Kittel, A. Enhanced near-field heat flow of a monolayer dielectric island. *Phys. Rev. Lett.* **110,** 134302 (2013).
7. Sadat, S., Meyhofer, E. & Reddy, P. Resistance thermometry-based picowatt-resolution heat-flow calorimeter. *Appl. Phys. Lett.* **102,** 163110 (2013).
8. Challener, W. A. *et al.* Heat-assisted magnetic recording by a near-field transducer with efficient optical energy transfer. *Nature Photon.* **3,** 220–224 (2009).
9. Pendry, J. B. Radiative exchange of heat between nanostructures. *J. Phys. Condens. Matter* **11,** 6621–6633 (1999).
10. Otey, C., Lau, W. T. & Fan, S. Thermal rectification through vacuum. *Phys. Rev. Lett.* **104,** 154301 (2010).
11. Rodriguez, A. W. *et al.* Frequency-selective near-field radiative heat transfer between photonic crystal slabs: a computational approach for arbitrary geometries and materials. *Phys. Rev. Lett.* **107,** 114302 (2011).
12. Guha, B., Otey, C., Poitras, C. B., Fan, S. H. & Lipson, M. Near-field radiative cooling of nanostructures. *Nano Lett.* **12,** 4546–4550 (2012).
13. Van Zwol, P. J., Ranno, L. & Chevrier, J. Tuning near field radiative heat flux through surface excitations with a metal insulator transition. *Phys. Rev. Lett.* **108,** 234301 (2012).
14. Ben-Abdallah, P. & Biehs, S. A. Near-field thermal transistor. *Phys. Rev. Lett.* **112,** 044301 (2014).
15. Polder, D. & Hove, M. A. V. Theory of radiative heat transfer between closely spaced bodies. *Phys. Rev. B* **4,** 3303–3314 (1971).
16. Joulain, K., Mulet, J-P., Marquier, F., Carminati, R. & Greffet, J-J. Surface electromagnetic waves thermally excited: radiative heat transfer, coherence properties and Casimir forces revisited in the near field. *Surf. Sci. Rep.* **57,** 59–112 (2005).
17. Volokitin, A. I. & Persson, B. N. J. Near-field radiative heat transfer and noncontact friction. *Rev. Mod. Phys.* **79,** 1291–1329 (2007).
18. Basu, S., Zhang, Z. & Fu, C. Review of near-field thermal radiation and its application to energy conversion. *Int. J. Energ. Res.* **33,** 1203–1232 (2009).
19. Biehs, S. A. Thermal heat radiation, near-field energy density and near-field radiative heat transfer of coated materials. *Eur. Phys. J. B* **58,** 423–431 (2007).
20. Francoeur, M., Menguc, M. P. & Vaillon, R. Coexistence of multiple regimes for near-field thermal radiation between two layers supporting surface phonon polaritons in the infrared. *Phys. Rev. B* **84,** 075436 (2011).
21. Basu, S. & Zhang, Z. M. Ultrasmall penetration depth in nanoscale thermal radiation. *Appl. Phys. Lett.* **95,** 133104 (2009).
22. Ganjeh, Y. *et al.* A platform to parallelize planar surfaces and control their spatial separation with nanometer resolution. *Rev. Sci. Instrum.* **83,** 105101 (2012).
23. Cahill, D. G. *et al.* Nanoscale thermal transport. II. 2003–2012. *Appl. Phys. Rev.* **1,** 011305 (2014).
24. Rytov, S. M., Kravtsov, I. A. & Tatarskii, V. I. *Principles of Statistical Radiophysics* 2nd edn, Vol. 3 (Springer-Verlag, 1987).
25. Whittaker, D. M. & Culshaw, I. S. Scattering-matrix treatment of patterned multilayer photonic structures. *Phys. Rev. B* **60,** 2610–2618 (1999).
26. Derjaguin, B. V., Abrikosova, I. I. & Lifshitz, E. M. Direct measurement of molecular attraction between solids separated by a narrow gap. *Q. Rev. Chem. Soc.* **10,** 295–329 (1956).
27. Biehs, S. A., Rousseau, E. & Greffet, J. J. Mesoscopic description of radiative heat transfer at the nanoscale. *Phys. Rev. Lett.* **105,** 234301 (2010).
28. Francoeur, M., Menguc, M. P. & Vaillon, R. Near-field radiative heat transfer enhancement via surface phonon polaritons coupling in thin films. *Appl. Phys. Lett.* **93,** 043109 (2008).
29. Rodriguez, A. W. *et al.* Anomalous near-field heat transfer between a cylinder and a perforated surface. *Phys. Rev. Lett.* **110,** 014301 (2013).
30. Lenert, A. *et al.* A nanophotonic solar thermophotovoltaic device. *Nature Nanotech.* **9,** 126–130 (2014).

Acknowledgements

P.R. and E.M. acknowledge support from the Army Research Office (W911NF-12-1-0612; device fabrication) and the National Science Foundation (CBET 1235691; instrumentation and measurements). J.C.C. acknowledges financial support from the Spanish MICINN (contract no. FIS2011-28851-C02-01) and thanks E. Moreno for helpful discussions. V.F-H. acknowledges financial support from 'la Caixa' Foundation. F.J.G-V. and J.F. acknowledge support from the European Research Council (ERC-2011-AdG proposal no. 290981). The authors acknowledge the Lurie Nanofabrication Facility (LNF) for facilitating the nanofabrication of devices.

Author contributions

The work was conceived by P.R. and E.M. The experiments were performed by B.S., Y.G. and A.F. under supervision by E.M. and P.R. The devices were designed and fabricated by S.S., D.T. and B.S. Modelling was performed by V.F-H. and J.F. under the supervision of F.J.G-V. and J.C.C. The manuscript was written by P.R., E.M. and J.C.C. with comments and input from all authors.

Additional information

Supplementary information is available in the online version of the paper. Reprints and permissions information is available online at www.nature.com/reprints. Correspondence and requests for materials should be addressed to P.R. and E.M.

Competing financial interests

The authors declare no competing financial interests.